Original scientific paper

THE IMPACT OF FINITE DIMENSIONS ON THE SENSING PERFORMANCE OF TERAHERTZ METAMATERIAL ABSORBER

Anja Kovačević, Milka Potrebić, Dejan Tošić

University of Belgrade, School of Electrical Engineering, Belgrade, Serbia

Abstract. *This paper investigates the impact of finite number of unit cells on the sensing performance of chosen THz metamaterial absorber. Sensor models with different number of unit cells varying from 16 to infinite have been created using WIPL-D software. The results of comparison show that as the sensor's size increases, its absorption response becomes more similar to the one of an infinite sensor structure. Metamaterial absorber with 50 unit cells expresses the similar behavior in terms of the corresponding frequency and amplitude shifts as the infinite absorber when the H9N2 virus sample of variable thickness is uniformly deposited on the top of the sensors' surface. The uneven distribution of sample affects the sensor's absorption response which has been proven on the example of sensor with 50 unit cells.*

Key words: *THz metamaterial absorber, finite dimensions, absorption response, H9N2 virus sample*

1. INTRODUCTION

Various metamaterials have been artificially designed to manipulate electromagnetic (EM) waves in the manner that enables their functional use in a wide range of device applications such as in switches, modulators, filters and sensors [1]. Basically, metamaterials are structures with periodic sub-wavelength metallic [1] or dielectric [2, 3] patterns that possess EM properties that are not found in natural materials [2]. Metamaterial metallic-based structures inherently have dissipation losses which can be used to enhance their absorption capabilities [1].

Metamaterial absorbers (MA) are devices that can minimize the reflection and theoretically eliminate transmission of the incident EM wave [4]. They are typically designed as metal-dielectric-metal structures [1, 5–7], but other possible designs include dielectric grating-based structures [4], integrated microfluidic structures [8] and dielectric-metal structures [2]. MAs can be used in solar power harvesting, material detection, thermal imaging and sensing [4].

MAs that work in terahertz (THz) domain are crucial for bio-sensing applications since the vibration resonances of biomolecules coincide with the THz range [9]. Besides that, THz technology has several different advantages relevant for the field of bio-sensing such as non-ionizing property and strong penetration capability [10]. Sensors based on THz MA can be used to detect various virus subtypes with wide range of particle size [11].

Since the physically realizable sensor has finite dimensions and therefore its structure cannot be fully periodical, we wanted to investigate the impact of finite number of unit cells on the sensing performance. First, we had to come up with proper modelling technique for both the infinite and finite sensor structure in WIPL-D software. The whole modelling process alongside the geometrical and material properties of the chosen THz MA will be described in Section 2. In Section 3, the obtained results that describe the behavior of modelled sensor structures with and without the sample will be presented and thoroughly discussed including the case when the sample is unevenly spread across the MA's surface.

2. SENSOR DESIGN AND MODELLING PROCESS

For the purpose of investigating the impact of finite dimensions on sensing performance, we have selected quad-band metamaterial absorber presented in [5]. The chosen MA is a typical planar metal-dielectric-metal structure whose quad-band absorption is achieved by introducing slight deformation to the traditional rectangular metallic resonator rather than using multiple single-band resonators of different sizes. Although there are four resonant frequencies, we will focus our analysis on the range of the first resonant frequency which is below 1 THz, but the concept can be broadened to the higher frequencies.

2.1. Unit Cell and Modelling of Infinite Sensor Structure

The unit cell structure is composed of metallic ground layer and perforated metallic resonator separated by a polyimide lossy dielectric spacer. The dimensions of interest are given in Figure 1. Both metallic layers are made of gold whose conductivity varies with the increase of frequency, but since the frequency range of interest is below 1 THz, the fixed value of 40.9 MS/m used in [5] is sufficient for obtaining good-quality results. If the analysis is to be extended to the range of higher frequencies, variation of conductivity can be taken into account by using Drude model [12]. In addition, the ground layer is thicker than the skin depth in the whole frequency range of interest which is essential for proper isolation between the substrate and the sensor itself.
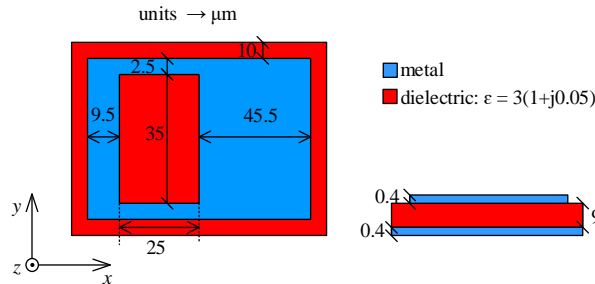

Fig. 1 THz MA unit cell with given dimensions

Metamaterials are composed of a large number of meta-atoms represented by unit cells. Consequently, the proper model of an infinite MA structure implies creating an orthogonal lattice of unit cells through the periodical repetition along the *x*- and *y*-axes which can be achieved by using periodic boundary conditions (PBC).

PBC are a set of boundary conditions applied for analysis of infinite 2D EM structures by using a single unit cell [13]. The modelling process of an infinite sensor structure in WIPL-D software using PBC option consists of three main steps.

Since PBC option is only available in scatterer operation mode, the first step is to choose an adequate scatterer mode. The bistatic radar cross-section (RCS) mode is more suitable for this particular structure considering the fixed position of field generator. Second step involves setting the values that define unit cell in terms of the occupying space and spatial repetition. X and Y values correspond to the start and end coordinates of the unit cell in *xy*-plane while the Z values are recommended to be set to 10% higher values than the cell size determined by its geometry [13]. Port 1 and 2 have been positioned at the top and on the bottom of the structure respectively. The last step consists of making planar unit cell structure by defining plates and their domains determined by the used materials and finally, specifying the source as a transverse electromagnetic (TEM) plane wave vertically irradiated to the sensor surface and the frequency range of interest. Additionally, the quality of planar structure model can be significantly improved by using imaging and edging.

2.2. Modelling of finite sensor structure

In order to create a model of finite sensor structure in WIPL-D, whole modelling process has to be done manually since the PBC option is no longer suitable which results in significantly higher time-consumption. Despite the introduced difficulties, the modelling of finite sensor has some significant advantages such as the ability to analyze the impact of the end effects which are inevitably present in the physically realizable structure and the possibility of modelling the uneven distribution of the sample across the sensor's surface which will be demonstrated in Section 3.

To fully investigate the impact of dimensions on sensor performance, we have created models for different numbers of unit cells (16, 50, 100 and 400). Although the expected dimensions of metamaterial biosensor device for experimental measurements are around 12 mm x 12 mm [14] which is equivalent to 24000 unit cells of the sensor observed in this paper, the THz source is usually focused on a much smaller area of the metamaterial sensor (approximately 1 mm^2 [15] which is equivalent to around 167 unit cells). In order to improve the efficiency of simulations, we have exploited the symmetry of modelled structure and the excitation by using the symmetry plane in our models which has cut the number of unknowns around two times without compromising the results of numerical calculations. The simulation frequency range was set to the frequency range of the first resonant peak of the infinite structure. The example of modelling a sensor of finite dimensions is given for structure made of 50 cells in Figure 2.
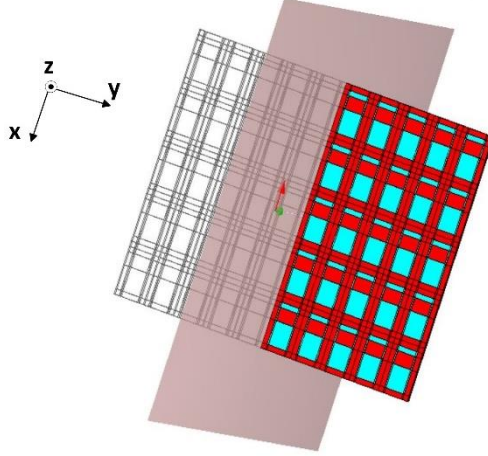
Fig. 2 Modelling of the sensor with 50 unit cells (the pink plane represents the used symmetry plane)

Main difficulty that has occurred during the modelling process is how to adequately define sensor ports so that the results can be compared with the previously obtained results for an infinite structure. The main goal is to determine the scattering parameters of sensor which can be achieved by mimicking the process that has been incorporated into the functioning of PBC option. Due to the existence of ground plane (Figure 1), the transmission coefficients s_{21} and s_{12} are practically brought down to zero. For that reason, in order to reduce the complexity of analysis, we have observed only s_{11}. By definition $|s_{11}|$ is:

$$|s_{11}| = \sqrt{\frac{P_{\text{refl}}}{P_{\text{inc}}}} \tag{1}$$

where P_{refl} and P_{inc} are powers of reflected and incident wave that had to be calculated in order to determine s_{11}. It should be noted that the definition (1) is valid only on condition that s_{12} is equal to zero which has been fulfilled. To calculate these powers, we have simulated the near field distribution in the plane parallel to the sensor's surface.

The power of the wave can be calculated by using complex Poynting vector $\mathbf{S}$:

$$P = \text{Re}\left\{ \int_{S'} \mathbf{S} \cdot d\mathbf{S}' \right\} = \text{Re}\left\{ \int_{S'} (\mathbf{E} \times \mathbf{H}^*) \cdot d\mathbf{S}' \right\} \tag{2}$$

where $\mathbf{E}$ and $\mathbf{H}$ are field vectors described by their x, y and z components and $d\mathbf{S}' = dS' \mathbf{i}_z$ is vector of the infinitely small surface dS'.

After arranging expression (2), it is necessary to perform its discretization since the analysis has been conducted in a finite number of points $n = N_x \cdot N_y$:

$$P = \text{Re}\left\{\Delta S' \sum_{n} (E_x H_y^* - E_y H_x^*)\right\} \tag{3}$$

where N_x and N_y are number of points along x- and y-axes in which the near field distribution has been calculated and $\Delta S' = S' / n$ is an elementary surface of the observed surface S'. We have assumed that all the surfaces $\Delta S'$ are equal and small enough so that the field distribution is approximately constant within them. In order to find the optimal n which supports this assumption, we have varied the total number of points in which the near field distribution is calculated from 441 to 10201. We have concluded that increasing number of points doesn't lead to the significant variations in the results. Therefore, we have set the total number of points to 441 for structures of 16 and 50 cells, 1681 for 100 cells and 3721 for 400 cells.

In order to get the near field distribution for the incident wave, we have created separate model with a single wire that doesn't have significant impact on the field. The incident wave only has E_x and H_y components onwards marked as E_{x0} and H_{y0}, thus simplifying power formula (3) to:

$$P_{\text{inc}} = -\text{Re}\left\{\Delta S' \sum_{n} (E_{x0} H_{y0}^*)\right\} \tag{4}$$

Minus sign has been added as the incident waves enters the surface.

For calculating the power of reflected wave, we have used the field components imported from the sensor model from which we have subtracted the field components of incident wave to obtain the fields of reflected wave E_{ir} and H_{ir} ($i = x, y$):

$$P_{\text{refl}} = \text{Re}\left\{\Delta S' \sum_{n} (E_{xr} H_{yr}^* - E_{yr} H_{xr}^*)\right\} \tag{5}$$

Finally, we have used (1) to determine $|s_{11}|$ for different frequencies from the operating range. Considering that the selected sensor was designed as MA, we have chosen the absorption as a reference parameter in our analysis. Since the transmission through the structure is negligible due to the existence of ground plane, the absorption of the chosen MA is fully defined through the reflection described by s_{11}:

$$A = 1 - |s_{11}|^2 \tag{6}$$

where $|s_{11}|^2$ is normalized reflected power.

2.3. Sample

To investigate the sensing capabilities of both infinite and finite sensor structures, we have chosen the sample of H9N2 subtype of Influenza A virus (IAV). IAVs are respiratory viruses with RNA genome and a serious possibility of causing human epidemics or pandemics [16]. Virus sample has been modeled as a continuous dielectric layer that completely covers the top of the MA structure. The complex permittivity of the sample has been determined by the frequency-dependant dispersive refractive index ($\tilde{n} = n + jk$) derived from the Drude-Lorentz model

$$n = \sqrt{\varepsilon} = \sqrt{1.5^2 - \frac{\omega_p^{\,2}}{\omega^2 - \omega_0^{\,2} + j\omega\gamma}} \qquad (7)$$

where $\omega_p = 4$ THz is the plasma frequency, $\omega_0 = 2.8\pi$ THz is the resonant frequency and $\gamma = 4$ THz is the damping coefficient [17]. Calculated $\tilde{n}$ for certain frequency from the operating frequency range has been modified with coefficients A and B retrieved by THz spectroscopy for H9N2 sample of protein concentration 0.28 mg/ml into the form of complex refractive index $An + B\, jk$ where $A = 1.2$ and $B = 1.4$ [17]. Finally, the complex permittivity required by WIPL-D software was calculated by squaring the corresponding complex refractive index. The whole process was repeated for each frequency used in simulation. It should be noted that coefficients A and B and therefore calculated values for complex permittivity of the sample refer to the specific protein concentration and may vary if it is changed. Therefore, the samples of different concentrations can be treated as completely different sample types. During the analysis, we have varied the thickness of virus layer to examine the sensors' behavior with different quantities of the deposited sample. The same analysis can be conducted for a different virus type by altering the coefficients A and B in addition to the parameters of Drude-Lorentz model given in (7). For example, for IAV subtypes H1N1 and H5N2, the Drude-Lorentz parameters remain the same as for H9N2, but the coefficients A and B have to be modified to (1, 1.4) and (1, 1) respectively [17].

3. RESULTS AND DISCUSSION

The results for selected THz MA are presented and discussed with the aim of investigating the effect that finite dimensions have on sensor's properties and sensing capabilities.

3.1. Behavior without the sample

The absorption response of a finite sensor structure obtained in the frequency range of the first peak significantly varies with the change of number of unit cells (Figure 3). As the number of cells increases, the peak width and its resonant frequency decrease while the prominence of the peak increases resulting in the response that becomes more similar to the one of an infinite sensor structure. All of the peaks show strong absorption which can be contributed to the combination of two effects: the influence of the perforated metallic resonator and the Fabry-Pérot effect as a consequence of the multiple reflections between the metallic layers [18].

In order to further compare infinite and finite structures, the corresponding Q-factors have been calculated and presented in Table 1 alongside with other parameters of interest such as resonant frequency $f_{resonant}$, full-width at half-maximum (FWHM) and maximal absorption value (A_{max}). The values given in Table 1 numerically confirm conclusions made by observing Figure 3. The structure with 16 cells does not have enough prominent resonant peak to determine FWHM and Q-factor. As the number of unit cells increases, the sensor's performance in the frequency range of the first resonant peak enhances which can be seen through the increase of Q-factor. All of the made observations lead to a very important conclusion that the finite sensor structure with the sufficient number of unit cells can potentially give very approximate results to the ones that are theoretically obtained using the infinite sensor model.
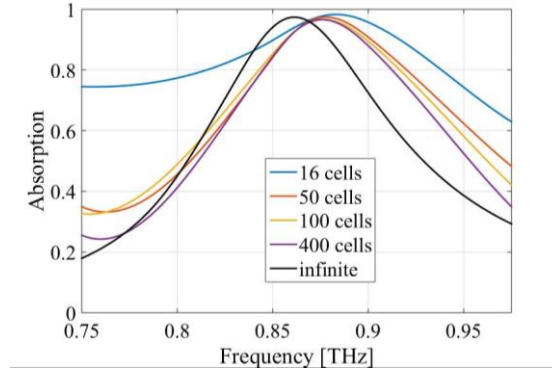
Fig. 3 Absorption response of the finite structure for different numbers of unit cells in comparison with the response of the infinite structure

Table 1 Numerical comparison of sensor models with different number of unit cells

Number of unit cells	$f_{resonant}$ [THz]	A_{max}	FWHM [THz]	Q-factor
16	0.883	0.983	/	/
50	0.878	0.9742	0.169	5.2
100	0.877	0.9662	0.166	5.2
400	0.876	0.9663	0.147	6
infinite	0.864	0.9741	0.127	6.8

To gain a better insight into the underlying physical mechanism of investigated sensor structures, we have calculated the distributions of electric and magnetic fields for both the infinite and finite sensor with 50 unit cells at their first resonant frequencies. The sensor with 50 unit cells has been chosen for further analysis since it has fewer unit cells than other models with prominent peaks which reduced total modelling and simulation time. The results are presented in Figure 4. Figure 4 (a) shows that the electric field calculated in the parallel plane close to the sensor's surface is mainly concentrated at the area around the resonator perforation. The electric field distribution is exactly the same for all the unit cells that compose the infinite sensor structure. On the contrary, Figure 4 (b) shows that the field distribution on the finite sensor's unit cell is dependent on its position in the structure. Mentioned phenomenon is the direct consequence of the finite dimensions of the sensor and the end effect that occurs on the borders of the structure. Figure 4 (c) and (d) show that the magnetic field distribution in the cross-section of both structures is fairly similar as the field is mainly gathered in the middle layer made of lossy dielectric. Such confinement of electromagnetic field is typical for the metal–dielectric–metal structures as shown in [8]. The field localization predominately affects the sensing performance as the placement of the sample should coincide with the strongest wave-matter interaction zone in order to achieve high sensitivity. Therefore, inverting the placement of the substrate and the sample has been proposed in an effort to enhance the interaction between the THz wave and the sample. MAs with integrated microfluidic channels based on this approach were built and tested with solutions of ethanol, glucose and bovine serum albumin (BSA) [8, 19]. However, it should be noted that, due to the technical difficulties during placing and removing samples, these

sensors may not be the most suitable candidates for applications that require large number of consecutive sensing tests and/or have samples that are not in the fully liquid form.
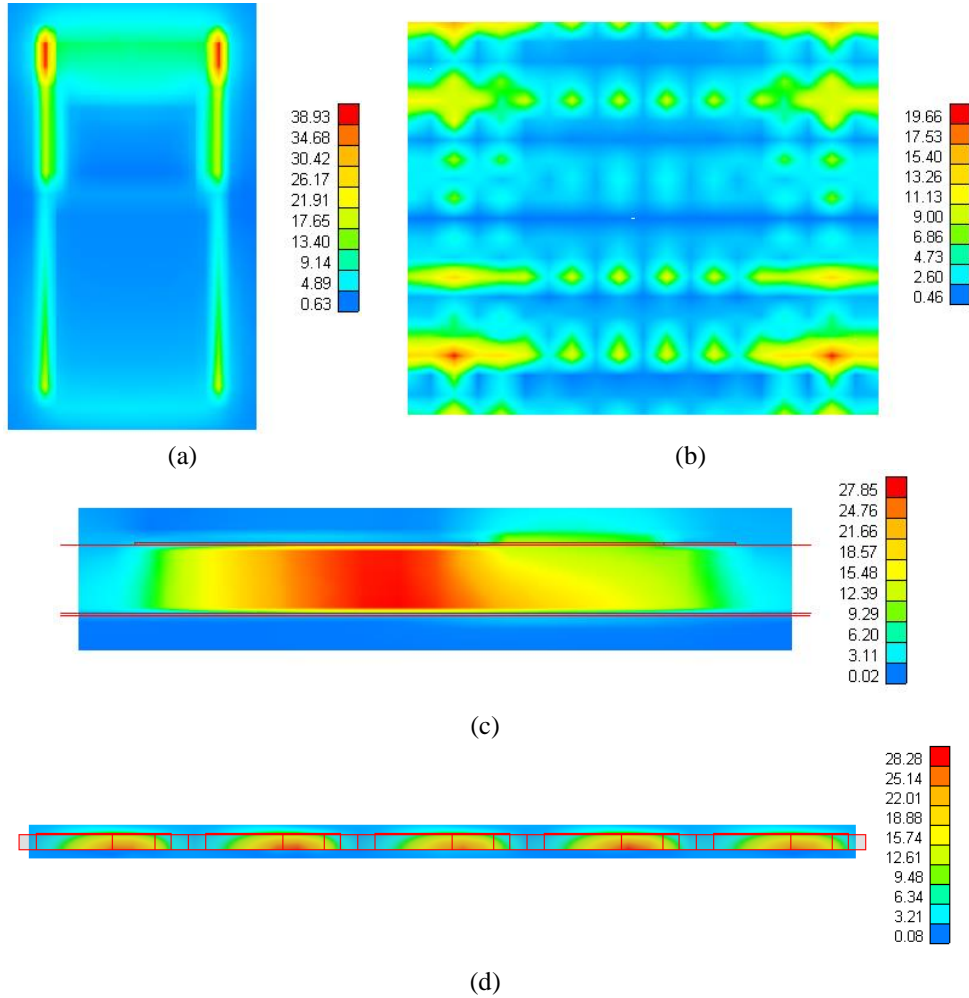

(a)   (b)

(c)

(d)

Fig. 4 Distribution of electric field [V/m] for (a) infinite and (b) finite sensor model and magnetic field [mA/m] for (c) infinite and (d) finite sensor model at the first resonant frequency

3.2. Behavior with the presence of sample

The example of absorption response of both structures in the frequency range of the first peak for three different thicknesses (*d*) of H9N2 is given in Figure 5. Both structures show the similar behavior with the presence of virus sample as the resonant peak shifts to the left when the thickness of the sample layer is increased. Consequently, the resonant frequency shift can be used not only as an indicator of the virus presence in the sample, but

also to determine the sample thickness. Figure 5 also suggests that there is a certain limit in such detection because of the frequency shift saturation that the resonant peak undergoes when the sample thickness is increased to a certain extent.

Beside the frequency, the resonant peak amplitude also varies with the modification of sample properties as shown in Figure 5. The values of both frequency and amplitude shifts for different thicknesses of the sample deposited on top of the both sensor structures are presented in Table 2. It should be noted that, unlike the resonant frequency that never grows when the thickness of the sample increases, the resonant peak amplitude sometimes grows and sometimes declines. In that sense, the values for amplitude shifts given in Table 2 are absolute values. Table 2 shows that the resonant peak of the absorption response that corresponds to the finite structure experiences larger frequency shifts and saturates faster compared to the one of the infinite structure. Additionally, the amplitude shifts are also more dynamic for the finite structure.
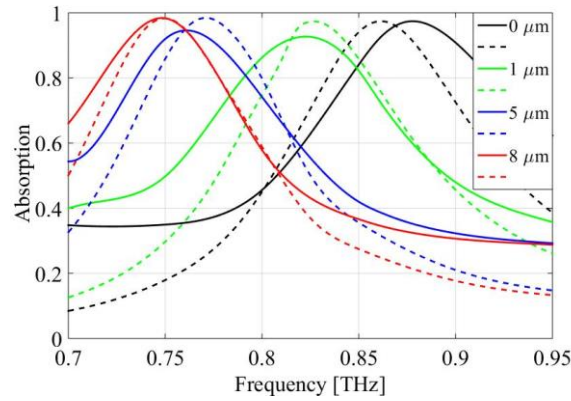

Fig. 5 Comparison between the absorption responses of the finite sensor made of 50 unit cells with different thicknesses of H9N2 sample (full line) and the results for the infinite model (dashed line)

Table 2 Frequency and amplitude shifts for different thicknesses of H9N2 sample deposited on top of the infinite and finite sensor structures

Structure	Thickness [μm]	$f_{resonant}$ [THz]	A_{max}	Frequency shift [GHz]	Amplitude shift [x10^{-4}]
Infinite	0	0.864	0.9741	0	0
	1	0.827	0.9736	37	5
	5	0.771	0.9844	93	103
	8	0.750	0.9828	114	87
Finite	0	0.878	0.9741	0	0
	1	0.823	0.9268	55	473
	5	0.761	0.9458	117	283
	8	0.748	0.9840	130	99

The previously conducted analysis refers to the uniform distribution of the virus sample across the sensors' surface. In order to investigate the impact of uneven sample distribution

on the response, we have created several models with different sample distributions based on the model of sensor with 50 unit cells. These models have been created by removing the sample from certain unit cells thus creating the "holes" in the sample layer. Since the observed structure has 50 unit cells, there are 2^{50} different distributions that can be analyzed (each unit cell can be covered with the sample or not). Taking into account the symmetry plane used in the modelling process shown in Figure 2, the number of possible distributions decreases to 2^{25} which is still considerable number to cover by analysis. In order to find the representative distributions to include into our models, we have set three possible parameters that have impact on the absorption response we wanted to characterize: the number of "holes", the separation between them and their position in terms of the field distribution given in Figure 4.

Let us first formalize the coordinates that describe the position of the "hole" in the sample placed on the top of the sensor's surface as in Figure 6. The gray unit cells from Figure 6 belong to the part of the structure that is obtained by using symmetry plane. We can only choose the position of the "hole" from one of the white unit cells and that choice will automatically place another "hole" on the symmetrical gray unit cell. For example, if the "hole" is placed on (2, 3), it will also inevitably be placed on (2, -3). Having that in mind, in the following analysis we will only declare the position of the "hole" from the white part of the structure and the position of the corresponding "hole" from the gray part will be implied. The number of "holes" will thus always be even.

(1,-5)	(1,-4)	(1,-3)	(1,-2)	(1,-1)	(1,1)	(1,2)	(1,3)	(1,4)	(1,5)	y
(2,-5)	(2,-4)	(2,-3)	(2,-2)	(2,-1)	(2,1)	(2,2)	(2,3)	(2,4)	(2,5)	
(3,-5)	(3,-4)	(3,-3)	(3,-2)	(3,-1)	(3,1)	(3,2)	(3,3)	(3,4)	(3,5)	
(4,-5)	(4,-4)	(4,-3)	(4,-2)	(4,-1)	(4,1)	(4,2)	(4,3)	(4,4)	(4,5)	
(5,-5)	(5,-4)	(5,-3)	(5,-2)	(5,-1)	(5,1)	(5,2)	(5,3)	(5,4)	(5,5)	

x

Fig. 6 The coordinates of the "holes" in the sample

First, the number of "holes" was set to two and their position and mutual distance were varied. The results presented in Figure 7 indicate that placing two "holes" in the sample does lead to certain changes in the absorption response such as small frequency and amplitude shifts and slight deformations of the resonant peak's shape. Both the amplitude and the frequency of the resonant peak increase when two "holes" in the sample are introduced. The maximum increase for both parameters is achieved in the case of two

connected "holes" in the center of the structure ((3, 1) and its pair), corresponding maximal frequency and amplitude shifts are 3 GHz and 0.0074. The changes of resonant frequencies and amplitudes are the smallest when the "holes" are further away from the center whether the "holes" are connected ((5, 1) and its pair) or completely separated from each other ((4, 4), (2, 3) and their pairs). The differences between the absorption values for models with "holes" in the sample and the original model with uniform distributions indicate that the shape of the resonant peak is slightly altered with the introduction of two "holes".
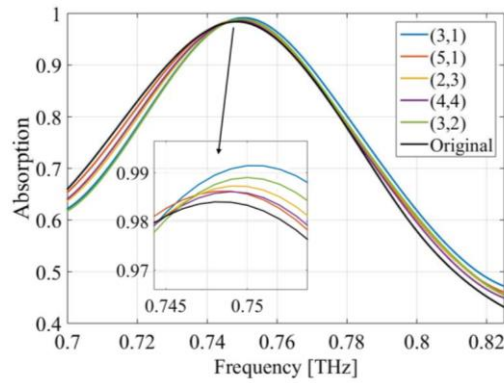

Fig. 7 Absorption response for different positions of the "holes" in the 8 µm thick sample in the case of two "holes"

Next, the number of "holes" was increased to six and three different distributions were observed. The obtained results are shown in Figure 8. The changes in the absorption response are more pronounced than when there were two "holes". The maximal frequency shift of 8 GHz is achieved when there are six consecutive "holes" forming a 1x6 rectangular "hole" near the center of the structure ((2, 1 – 3) and their pairs). The peak amplitude for that case has the maximal decrease of 0.0221 which is about three times the absolute value
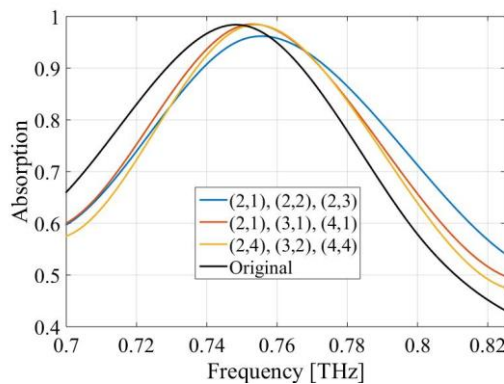

Fig. 8 Absorption response for different positions of the "holes" in the 8 µm thick sample in the case of six "holes"

of the corresponding shift for the two "holes". In other two cases, the peak amplitude is slightly increased, but significantly less than for the two "holes" in the sample.

4. CONCLUSION

We have thoroughly investigated the impact of finite dimensions on the sensing performance of the THz metamaterial absorber based on the typical planar metal-dielectric-metal structure. The results have shown that as the number of unit cells increases, the absorption response approaches the one of an infinite structure which is numerically reflected in the decreased width of the resonant peak and the increased Q-factor. The calculated electric field distribution has indicated that the field was mainly localized around the rectangular perforation regardless of the number of unit cells. Unlike the infinite structure, the structure with finite number of unit cells has shown the dependency of the field distribution on the position of the unit cell due to the presence of the end effect. The electromagnetic field was primarily confined in the lossy dielectric layer for both the infinite and the finite structure which is typical for metal-dielectric-metal based structures.

The behavior of the infinite and finite sensors in the presence of the H9N2 virus sample was examined. First, the sample was evenly distributed across the sensors' surfaces. The results have shown that the resonant peak of the finite structure experiences greater frequency shifts and saturates more quickly with the increase of the virus layer thickness in comparison with the infinite structure. Finally, we investigated the effect of uneven sample distribution on the finite sensor structure by removing the sample from the top of the certain unit cells. The analysis has shown that creating "holes" in the sample does lead to changes in the absorption response such as frequency and amplitude shifts and slight deformations of the resonant peak's shape. The number of "holes" in the sample is proven to be the parameter that contributes to the mentioned changes the most.

REFERENCES

[1]   B. X. Wang, W. Q. Huang and L. L. Wang, "Ultra-narrow terahertz perfect light absorber based on surface lattice resonance of a sandwich resonator for sensing applications", *RSC Advances*, vol. 7, pp. 42956-42963, 2017.

[2]   D. Hu, T. Meng, H. Wang, Y. Ma and Q. Zhu, "Ultra-narrow-band terahertz perfect metamaterial absorber for refractive index sensing application", *Results in Phys.*, vol. 19, p. 103567, pp. 1-5, 2020.

[3]   Y. Wang, D. Zhu, Z. Cui, L. Hou, L. Lin, F. Qu, X. Liu and P. Nie, "All-Dielectric Terahertz Plasmonic Metamaterial Absorbers and High-Sensitivity Sensing", *ACS Omega*, vol. 4, pp. 18645-18652, 2019.

[4]   F. Yan, Q. Li, H. Tian, Z. Wang and L. Li, "Ultrahigh Q-factor dual-band terahertz perfect absorber with dielectric grating slit waveguide for sensing", *J. Phys. D: Appl. Phys.*, vol. 53, p. 235103, pp. 1-9, 2020.

[5]   Q. Xie, G. Dong, B. Wang and W. Huang, "Design of Quad-Band Terahertz Metamaterial Absorber Using a Perforated Rectangular Resonator for Sensing Applications", *Nanoscale Res. Lett.*, vol. 13, p. 137, pp. 1-8, 2018.

[6]   M. Janneh, A. de Marcellis, E. Palange, A. T. Tenggara and D. Byun, "Design of a metasurface-based dual-band Terahertz perfect absorber with very high Q-factors for sensing applications", *Optics Commun.*, vol. 416, pp. 152-159, 2018.

[7]   W. Yin, Z. Shen, S. Li, L. Zhang and X. Chen, "A Three-Dimensional Dual-Band Terahertz Perfect Absorber as a Highly Sensitive Sensor", *Front. Phys.*, vol. 9, p. 665280, pp. 1-10, 2021.

[8]   X. Hu, G. Xu, L. Wen, H. Wang, Y. Zhao, Y. Zhang, D. R. S. Cumming and Q. Chen, "Metamaterial absorber integrated microfluidic terahertz sensors", *Laser Photonics Rev.*, vol. 10, pp. 962-969, 2016.

[9]   L. Cong, S. Tan, R. Yahiaoui, F. Yan, W. Zhang and R. Singh, "Experimental demonstration of ultrasensitive sensing with terahertz metamaterial absorbers: A comparison with the metasurfaces", *Appl. Phys. Lett.*, vol. 106, p. 031107, pp. 1-7, 2015.

[10] A. Kovačević, M. Potrebić and D. Tošić, "Sensitivity Analysis of Possible THz Virus Detection Using Quad-Band Metamaterial Sensor", In Proceedings of the IEEE 32nd International Conference on Microelectronics (MIEL), Niš, Serbia, 2021, pp 107-110.

[11] N. Akter, M. M. Hasan and N. Pala, "A Review of THz Technologies for Rapid Sensing and Detection of Viruses including SARS-CoV-2", *MDPI Biosensors*, vol. 11, p. 349, pp. 1-21, 2021.

[12] N. Shen, P. Tassin, T. Koschny and C. Soukoulis, "Comparison of gold- and graphene-based resonant nano-structures for terahertz metamaterials and an ultra-thin graphene-based modulator", *Phys. Rev. B,* vol. 90, no. 11, p. 115437, pp. 1-8, 2014.

[13] WIPL-D Pro 17, 3D Electromagnetic Solver, WIPL-D d.o.o., Belgrade, Serbia, 2021. Available online: http://www.wipl-d.com (accessed on 29 April 2022).

[14] G. Wang, F. Zhu, T. Lang, J. Liu, Z. Hong and J. Qin, "All-metal terahertz metamaterial biosensor for protein detection", *Nanoscale Res. Lett.*, vol. 16, p. 109, pp. 1-10, 2021

[15] S. J. Park, S. H. Cha, G. A. Shin and Y. H. Ahn, "Sensing viruses using terahertz nano-gap metamaterials", *Biomed. Opt. Express*, vol. 8, pp. 3551-3558, 2017.

[16] B. Dadonaite, B. Gilbertson, M. L. Knight, S. Trifković, S. Rockman, A. Laederach, L. E. Brown, E. Fodor, D. L. V. Bauer, "The Structure of the Influenza A Virus Genome", *Nat. Microbiol.*, vol. 4, no. 11, pp. 1781-1789, 2019.

[17] M. Amin, O. Siddiqui, H. Abutarboush, M. Farhat and R. Ramzan, "A THz graphene metasurface for polarization selective virus sensing", *Carbon*, vol. 176, pp. 580-591, 2021.

[18] B. Wang, A. Sadeqi, R. Ma, P. Wang, W. Tsujita, K. Sadamoto, Y. Sawa, H. R. Nejad, S. Sonkusale, C. Wang et al, "Metamaterial Absorber for THz Polarimetric Sensing", In Proceedings of the SPIE, Terahertz, RF, Millimeter, and Submillimeter-Wave Technology and Applications XI, San Francisco, CA, USA, 2018, vol. 10531, pp. 1-7.

[19] F. Lan, F. Luo, P. Mazumder, Z. Yang, L. Meng, Z. Bao, J. Zhou, Y. Zhang, S. Liang, Z. Shi et al, "Dual-band refractometric terahertz biosensing with intense wave-matter-overlap microfluidic channel", *Biomed. Opt. Express*, vol. 10, pp. 3789-3799, 2019.